Available online at www.sciencedirect.com
ScienceDirect
Journal of Photochemistry and Photobiology A: Chemistry 185 (2007) 301–311
Journal of Photochemistry and Photobiology A:Chemistry
www.elsevier.com/locate/jphotochem

Photodriven reduction and oxidation reactions on colloidal semiconductor particles: Implications for prebiotic synthesis

Xiang V. Zhang [a], Shelby P. Ellery [a], Cynthia M. Friend [a,b], Heinrich D. Holland [c], F.M. Michel [d], Martin A.A. Schoonen [d], Scot T. Martin [a,*]

[a] *Division of Engineering and Applied Sciences, Harvard University, Cambridge, MA, United States*
[b] *Department of Chemistry & Chemical Biology, Harvard University, Cambridge, MA, United States*
[c] *Department of Earth and Planetary Sciences, Harvard University, Cambridge, MA, United States*
[d] *Department of Geosciences, State University of New York, Stony Brook, NY, United States*

Received 27 April 2006; received in revised form 22 June 2006; accepted 24 June 2006
Available online 14 August 2006

Abstract

Photoelectrochemical reactions on mineral surfaces may have contributed to the synthesis of prebiotic molecules on early Earth. Laboratory experiments were conducted to develop this idea. Colloidal particles of ZnS were selected as a prototypical semiconducting mineral material. We investigated (1) the capability of the ZnS colloid to reduce aqueous CO_2 under ultraviolet irradiation to yield formate in the presence of a sulfur hole scavenger and (2) to oxidize formate to yield CO_2 in the absence of a hole scavenger. In the presence of the hole scavenger, the initial quantum efficiency is 10% for formate production from CO_2 at pH 6.3. The reaction rate is sensitive to the pH of the solution, increasing with acidity for the pH range of 5–9. The initial formate production rate is proportional to the concentration of aqueous inorganic carbon from 13 to 65 mM, suggesting an absence of surface saturation. Photoproducts other than formate also form, including acetate and propionate, a finding which demonstrates the formation of carbon–carbon coupling products. In the absence of hole scavenger but in the presence of the ZnS colloid, formate is photooxidized with a quantum efficiency of 1.1%. The likely presence of semiconducting colloidal particles in the oceans of the prebiotic Earth suggests that photochemical reactions on their surfaces could have played a significant role in the synthesis of organic molecules.

Keywords: Early Earth; Origin of life; Carbon fixation; Zinc sulfide

1. Introduction

An unanswered question about the origins of life is the source of the organic molecules that constituted the foundational building blocks of self assembly and replication. Colloidal photochemistry, which has received limited attention in regard to this question, can open novel reaction pathways and speed reaction rates because of the chemistry of excited-state species. The operative principle is that an electron in the valence band is promoted to the conduction band when a semiconducting mineral absorbs a photon of energy greater than the bandgap [1]. The conduction-band electrons and the valence-band holes can drive reduction and oxidation reactions, respectively, thereby interconverting carbon through its oxidation states and hence synthesizing new organic molecules (Table 1 and Fig. 1).

Zinc sulfide, a semiconductor which occurs in nature as the minerals sphalerite and wurtzite, was chosen by us as a model photocatalyst for study because of its occurrence in Hadean marine environments and because the conduction-band electrons have a sufficiently negative reduction potential (−1.04 V versus NHE) to reduce CO_2 to $CO_2^{\bullet-}$ radical (Table 2). Small organic molecules such as formate result [2–4]. The $CO_2^{\bullet-}$ radical also undergoes chain addition to form C_2 and longer chain carbon–carbon compounds [5].

The valence-band holes of ZnS are sufficiently energetic (+2.56 V versus NHE) to oxidize a range of inorganic and organic molecules. As a result, under unfavorable reaction conditions, the reactions of ZnS can have a null reduction–oxidation cycle. Under favorable reaction conditions, however, useful net transformations can occur, such as reduction reactions that build

* Corresponding author. Tel.: +1 617 4957620.
E-mail address: scot_martin@harvard.edu (S.T. Martin).
URL: http://www.deas.harvard.edu/environmental-chemistry/.

1010-6030/$ – see front matter © 2006 Elsevier B.V. All rights reserved.
doi:10.1016/j.jphotochem.2006.06.025

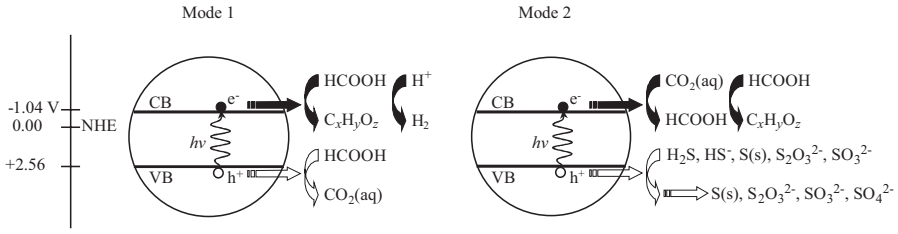

Fig. 1. Two modes of photodriven reduction and oxidation reactions on colloidal semiconductor particles. (left) Mode 1, photooxidation of formate to generate dissolved inorganic carbon. The electron scavenger is also formate. The overall reaction is formate disproportionation to dissolved inorganic carbon and carbon–carbon coupling products. (right) Mode 2, photoreduction of dissolved inorganic carbon to generate formate (HCOOH) and carbon–carbon coupling products ($C_xH_yO_z$). The hole scavenger is an aqueous sulfur solution.

Table 1
Common chemical carbon species and their oxidation states

Oxidation state	Species
+IV	$H_2CO_3^*$, HCO_3^-, CO_3^{2-} (sum is C_T^{+IV})
+II	HCOOH (formic acid), $HCOO^-$ (formate), and CO
0	$C_6H_{12}O_6$ (glucose) and HCHO (formaldehyde)
−II	CH_3OH (methanol)
−IV	CH_4 (methane)

up organic molecules while a sacrificial electron donor is oxidized. By harvesting the sun's energy, photocatalysis by semiconducting minerals can provide free energy for these reactions when necessary and, in addition, can cause rapid reactions rates because of high overpotentials. The bandgap of ZnS is 3.6 eV (344 nm).

Under the conditions of the prebiotic Earth some 4 Ga ago, ZnS was stable with respect to $ZnCO_3$ in regard to the interconversion reaction:

$$ZnS + H_2O + CO_2 \rightarrow ZnCO_3 + H_2S \quad (1)$$

Table 2
Reduction potentials for some half reactions of carbon and sulfur species

Reduction half-reaction	$E^0_{1/2}$ (V) (NHE)
$Ø_{ZnS} + e^- = e^-_{CB(ZnS^-)}$	−1.04
$2CO_2(g) + 2e^- = (COO^-)_2$ [oxalate]	−0.63
$CO_2(g) + H^+ + 2e^- = HCOO^-$ [formate]	−0.31
$SO_4^{2-} + 2e^- + 2H^+ = SO_3^{2-} + H_2O$	−0.10
$CO_2(g) + 4H^+ + 4e^- = HCHO(aq) + H_2O$	−0.071
$S(s, ortho) + 2e^- + 2H^+ = H_2S(aq)$	−0.053
$2H^+ + 2e^- = H_2$	+0.00
$CO_2(g) + 8H^+ + 8e^- = CH_4(g)$ [methane] + $2H_2O$	+0.017
$2CO_2(g) + 7H^+ + 8e^- = CH_3COO^-$ [acetate] + $2H_2O$	+0.075
$2SO_4^{2-} + 8e^- + 10H^+ = S_2O_3^{2-} + 5H_2O$	+0.29
$SO_4^{2-} + 8e^- + 10H^+ = H_2S(aq) + 4H_2O$	+0.30
$SO_4^{2-} + 6e^- + 8H^+ = S(s, ortho) + 4H_2O$	+0.36
$h^+_{VB(ZnS^+)} + e^- = Ø_{ZnS}$	+2.56

The table shows that photoexcited ZnS can reduce any of the species on the left-hand side of the equations and oxidize any of the species on the right-hand side of the equations. (Values are taken from Table 7.1 of F.M.M. Morel and J.G. Hering, *Principles and Applications of Aquatic Chemistry*, Wiley: New York, 1993, using the relation $E^0_{1/2} = 0.05916\,pe^0$. Reduction potentials are written for all species in their standard states and must be adjusted for calculations under actual reaction conditions.)

so long as $P_{H_2S} : P_{CO_2} > 1.3 \times 10^{-12}$. Current best estimates suggest $10^{-5} < P_{H_2S} : P_{CO_2} < 10^{-3}$ on the prebiotic Earth [6]. ZnS also has a low water solubility. Therefore, widespread occurrence of hydrothermal vents on the early Earth [7] may have led to colloidal ZnS and other semiconducting minerals of sufficient concentrations to lead to globally significant photochemical reactions in the euphotic layer of the prebiotic ocean.

In this paper, we report on the photoelectrochemistry of ZnS colloids. The photochemical processes are depicted in Fig. 1, and the reduction potentials of the half reactions of some carbon and sulfur species are given in Table 2. We use formic acid mineralization (mode 1) and CO_2 fixation (mode 2) as general probes of photoreactivity, leaving the question of specific chemical syntheses for future work. The reaction conditions in the current study (i.e., pH, ultraviolet wavelengths, photocatalyst, hole scavenger, and anoxic environment) were chosen to simulate the conditions on the prebiotic Earth. Earlier studies demonstrating photoelectrochemical conversion of CO_2 over ZnS were not performed under conditions relevant to early Earth [2,5,8–10].

The pH of the prebiotic ocean was probably between 5.5 and 8 [11,12], which is the same range as in our pH-dependent studies. There was very little oxygen in the prebiotic atmosphere. Sulfur was thus present largely as S^{-II} (i.e., sulfide H_2S and HS^-) rather than as S^{+VI} (i.e., sulfate SO_4^{2-}) [13]. A reduced sulfur solution, serving as a hole scavenger, was therefore used in our studies. The dissolved inorganic carbon content of the prebiotic ocean may have been 65 mM or higher for a CO_2 partial pressure of 1 atm in the atmosphere of early Earth. Therefore, we conducted concentration-dependent studies up to 65 mM.

2. Experimental

2.1. Preparation of ZnS colloidal suspensions

2.1.1. ZnS synthesis—method 1

ZnS colloidal suspensions were synthesized by two methods. In the first method, ZnS particles were prepared at 15 °C by mixing 250 mL of 50 mM $ZnSO_4$ (EM Science, Germany, 99.5% assay) with 250 mL of nominally 50 mM Na_2S (EMD Chemicals, 98% assay). The $ZnSO_4$ and Na_2S solutions were prepared by dissolving the solids in Ar-purged ultrapure water (18 MΩ cm). Na_2S is difficult to obtain in high purity because of

its susceptibility to oxidation, and the solution prepared nominally as 50 mM Na_2S actually had a smaller concentration of Na_2S and contained significant quantities of other dissolved sulfur oxyanions such as thiosulfate and sulfite. The concentration of S_T^{-II}, calculated as $S_T^{-II} = [H_2S(aq)] + [HS^-] + [S^{2-}]$, was assayed by a sulfide-sensitive electrode after preparation of the nominal solution.

Immediately after mixing together the $ZnSO_4$ and Na_2S solutions, a white colloidal suspension of ZnS formed at a loading of 2.3 g L^{-1}. The synthesis was carried out in an argon environment to avoid sample oxidation. The ZnS colloid suspension was used directly for the photochemical experiments, without rinsing or other preparation.

2.1.2. ZnS synthesis—method 2

In the second method, a ZnS colloidal suspension was synthesized by first mixing 500 mL of 0.2 M $ZnCl_2$ (Fisher Chemicals—99.7% assay) with 525 mL of nominally 0.2 M Na_2S (Fisher Chemicals—99.4% assay). The ZnS suspension was subsequently aged under anoxic conditions in a preheated water bath at 70 ± 2 °C for 142 h with gentle shaking [14]. The aging process was concluded by quenching for 30 min at 22 ± 2 °C. The supernatant of the ZnS colloidal suspension was decanted in an anoxic atmosphere. The resulting ZnS slurry was transferred into 50-mL centrifuge tubes and rinsed to remove NaCl. Except for the aging and the centrifuging of the ZnS, all other handling was conducted in an anoxic glovebox equipped with a palladium O_2-scrubbing catalyst and a digital H_2/O_2 analyzer (Coylabs). During aging, the sample was sealed in a Pyrex reaction vessel with a small anoxic headspace.

A protocol was developed for rinsing the slurry while avoiding the oxidation of ZnS. The ZnS slurry was centrifuged for 5 min at 5000 rpm, after which the supernatant was removed and 45 mL of 1 mM sodium sulfide rinse solution was added. The sulfide rinse solution also served as a scavenger of oxygen and thus prevented the surface oxidation of the ZnS precipitate. After the addition of the rinse solution, the ZnS slurry was resuspended by placing the centrifuge tubes in a vortexer for 20 s and a sonicator bath for 60 s. The centrifuge–decant–resuspend cycle was repeated four times. At the end of the rinsing process, the ZnS slurry was stored in a 250-mL Pyrex bottle wrapped in foil until needed for the photochemistry experiments.

The loading (grams of ZnS per liter slurry) of the ZnS slurry was determined using gravimetry. A 5-mL sample of each ZnS slurry was weighed to calculate the slurry density (g-slurry per L-slurry). The loading was then calculated using a water density of 1000 g-liquid per L-water and a solid density of 4100 g-ZnS per L-ZnS [15]. The loading varied among slurries from 39 to 57 g-ZnS per L-slurry. The slurry was diluted to 2.3 g L^{-1} for the photochemistry experiments.

Sample characterization is described in Appendix A.

2.2. Photochemistry experiments

2.2.1. Reactant mixture

Five hundred milliliters of a ZnS colloidal suspension, prepared by either method 1 or 2 at a loading of 2.3 g L^{-1}, was thoroughly mixed at pH 12 with 20 mL of 200 mM Na_2S (assayed) and placed into a photochemical reactor [16]. The Na_2S solution (8 mM after mixing) contained both aqueous H_2S and HS^- as well as other sulfur oxyanions, originating either as impurities in solid Na_2S or from rapid oxidation of HS^- by residual $O_2(aq)$. This solution served principally as a valence-band hole scavenger. It also ensured that anoxic conditions were maintained throughout the course of the experiment. The headspace of the reactor was filled with argon.

Inorganic carbon was introduced into the reaction mixture prior to irradiation by one of two alternative protocols, normally by bubbling CO_2 or in some cases by adding $NaHCO_3$. (1) Bubbling was done with Ultra High Purity CO_2 (99.99%, IGO Gases, MA) at a flow rate of 385 mL min^{-1} for 150 s, which reduced the pH of the reaction mixture from 12.0 to 6.3. Measurements with a sulfide-selective electrode (sensitive to S_T^{-II}), with ion chromatography, and a with total-inorganic-carbon analyzer showed that the initial reaction conditions were 2 mM HS^-, 1 mM $S_2O_3^{2-}$, 0.1 mM SO_3^{2-}, and 33 mM C_T^{+IV}, where $C_T^{+IV} = [H_2CO_3^*] + [HCO_3^-] + [CO_3^{2-}]$ and $[H_2CO_3^*] = [CO_2(aq)] + [H_2CO_3]$. Therefore, significant H_2S offgassing occurred during CO_2 bubbling (i.e., 8 mM S_T^{-II} decreased to 2 mM S_T^{-II}). For experiments using ZnS prepared from $ZnSO_4$ (i.e., method 1), 25 mM SO_4^{2-} was also present. (2) $NaHCO_3$ (EMD Chemicals, 99.7% assay) was added to the reactor while purging with argon, and the pH was subsequently adjusted to 6.3 or to another desired value with H_2SO_4 (EMD Chemicals, 98.0% assay). A third protocol was employed for formate-addition experiments, in which 1.4 mM sodium formate (Acros Organics, 99%) was added and no inorganic carbon was added.

Equilibrium calculations for a closed system (i.e., during irradiation) showed that the headspace contained negligible amounts of $H_2S(g)$ and $CO_2(g)$ compared to S_T^{-II} and C_T^{+IV}, even for the lowest pH studied of 5.3 [17]. In these calculations, the pK_a values employed were 7.0 for H_2S, 13.9 for HS^-, 6.35 for $H_2CO_3^*$, and 10.33 for HCO_3^-. The Henry's law constants were 9.8 atm M^{-1} H_2S and 28.8 atm M^{-1} for $H_2CO_3^*$.

2.2.2. Irradiation

The photochemical apparatus and the detailed experimental protocols were described earlier [16]. The ZnS colloidal suspensions were irradiated inside a sealed 500 mL photochemical reaction vessel at 288 K. The light intensity from the 450 W medium-pressure UV Hg arc lamp was 2.2×10^{-5} M s^{-1} (i.e., Einsteins s^{-1}) as measured by using potassium iron(III) oxalate actinometry. The light spectrum included photons having wavelengths from 200 to 400 nm. After exposure to UV irradiation for a selected time period, 1.0 mL of the colloidal suspension was withdrawn from the reaction vessel through a septum and then forced through a 0.2-μm syringe filter to remove particles. For sulfide analyses, the pH was immediately adjusted (see below). The withdrawn solutions were analyzed by ion chromatography (formate, acetate, propionate, thiosulfate, sulfite, and sulfate concentrations), sulfide-selective electrode (S_T^{-II}), atomic absorption spectroscopy (aqueous Zn^{2+}), and total organic carbon.

2.3. Chemical product analysis

Ion chromatography (Dionex DX120 with AS11-HC column, conductivity detector, self-regeneration suppression) was used to quantify anionic photochemical products, specifically formate, acetate, and propionate. For formate analysis, an eluent of 20 mM NaOH solution and a flow rate of 0.85 mL min^{-1} were employed. Thiosulfate, sulfite, and sulfate also eluted with this method. Aliquots were analyzed immediately after they were withdrawn from the photochemical apparatus. Acetate and propionate were also analyzed for some samples by employing an eluent of sodium borate (5 mM) at a flow rate of 1.50 mL min^{-1}. The species in solution were identified by comparison to the chromatograms of pure chemicals. The concentrations were obtained by calibration with a series of standard solutions.

The total organic carbon (TOC) content of some aliquots was determined by Huffman Laboratory, Colorado, up to two weeks after collection from the photochemical apparatus. Standard Method 5310C was used for the analysis [18]. The aliquots were acidified to pH 1 at Huffman Laboratory and were purged to release CO_2 to the gas phase. The amount of CO_2 released (i.e., total inorganic carbon (TIC)) was quantified by infrared detection. After the removal of inorganic carbon, the aliquot was oxidized by a hot persulfate solution, converting the organic carbon to CO_2. The sample was again purged, and the amount of CO_2 released yielded the total organic carbon. The detection limit was 0.2 mg-carbon L^{-1}.

Total S(−II) concentration S_T^{-II} was measured using a sulfide-selective electrode (Orion 96–16 Ionplus™ Silver/Sulfide electrode). For these measurements, 2.0 mL aliquots withdrawn from the photochemical apparatus were immediately mixed with 2.0 mL of 2.0 M NaOH to obtain a pH of 14, thereby minimizing offgassing of H_2S, although some minimal loss certainly occurred. The electrode was calibrated with alkaline Na_2S solution standards.

The aqueous Zn^{2+} concentrations of withdrawn samples were measured by atomic absorption spectroscopy (AAnalyst 300 atomic absorption spectrometer equipped with an HGA 850 graphite furnace attachment; Perkin-Elmer, Shelton, CT). Analytical standards read during analysis were within 10% of the known concentrations. Under our analytical conditions, the limit of detection for this technique was 2 nM.

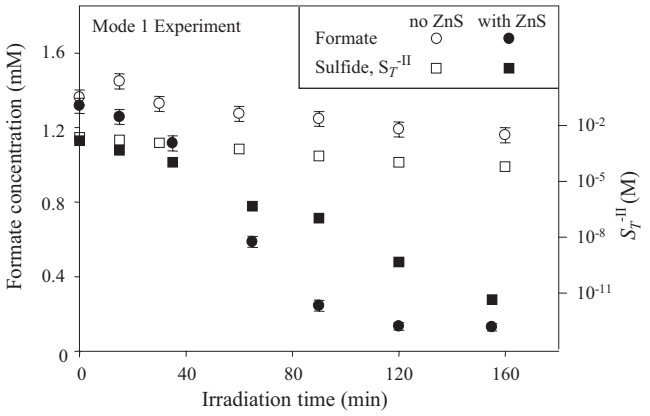

Fig. 2. Time profile of formate and S_T^{-II} concentrations during irradiation in the presence and absence of ZnS (mode 1 experiment). The initial solution is spiked in both cases with 1.4 mM sodium formate. No inorganic CO_2 is added to the solution. *Initial conditions*: 2.3 g L^{-1} ZnS (method 1), 2 mM sulfur hole scavenger, pH 6.3, 15 °C, and ultraviolet irradiation (200–400 nm).

3. Results and discussion

3.1. Formate loss: photooxidation reactions with ZnS colloid

Formate is photodecomposed by ZnS once S_T^{-II} is depleted (Fig. 2), a process depicted by mode 1 in Fig. 1. Specifically, Fig. 2 shows that in the presence of ZnS particles the concentration of formate decreases rapidly for increasing irradiation time in a solution initially spiked with formate after an induction period of 45 min that depletes S_T^{-II}. Control experiments described by Table 3 demonstrate the occurrence of a heterogeneous photoelectrochemical reaction (namely, mode 1 of Fig. 1). The loss rate from homogeneous photolysis in the absence of ZnS colloid is at least twice as slow (control B). The homogeneous photolysis reactions are $HCOOH + h\nu \rightarrow CO + H_2O$ and $HCOOH + h\nu \rightarrow CO_2 + H_2$ [19]. No decrease of formate occurs in the dark when the irradiation is terminated after 45 min

Table 3
Control experiments to demonstrate the occurrence of a heterogeneous photoelectrochemical reaction (namely, mode 1 of Fig. 1) for the loss of formate in the presence of ultraviolet irradiation and colloidal ZnS particles and the absence of sulfur hole scavenger

Description	Variables				Observation
	UV (λ < 410 nm)	Catalyst (ZnS(s))	Absence of sulfur hole scavenger	Formate	Formate loss
Photochemical reaction 1	Yes	Yes	Yes	Yes	Yes (100%)
Control A	No	Yes	Yes	Yes	No
Control B	Yes	No	Yes	Yes	Slowed (50%)
Control C	Yes	Yes	No	Yes	No[a]
Control D	Yes	Yes	Yes	No	No[b]
Control E	Yes	No	No	Yes	Slow (5%)

Reaction conditions are described in the caption of Fig. 2. Percentages in parentheses indicate the relative initial rates.
[a] No formate loss until HS^- is exhausted after 40 min.
[b] Formate is not present within analytical uncertainty during irradiation.

(results not shown). The results therefore show that the heterogeneous loss of formate requires the presence both of ZnS colloid and light and is, therefore, photoelectrochemically driven.

Significant formate loss, beyond what can be explained by homogeneous photolysis screened by HS^- absorption (control E), begins only after S_T^{-II} is depleted from 10^{-4} to 10^{-6} M after 60 min of irradiation (Fig. 2). The implication is that significant formate homogeneous photolysis and heterogeneous photooxidation begin only once S_T^{-II} scavengers are depleted. S_T^{-II} is not fully converted to S^{+VI} at 60 min, however, because a yellow solid (sulfur) is visible in the colloid and the sulfate concentration continues to increase almost linearly after 60 min (data not shown).

The heterogeneous loss of formate is driven by photooxidation to CO_2. The results of the TOC analysis have a yield of no more than 0.22 mM of the initial of 1.3 mM formate. In a comparison experiment having no added sulfur hole scavenger ($S_T^{-II} < 10^{-10}$ M), 1.9 mM of formate is lost and 0.4 mM of TOC as carbon is formed (data not shown). We speculate that the balance of the electron scavenging in mode 1 is due to H^+ reduction to form H_2, although we did not analyze the products for the presence of H_2. According to Table 1, as an upper limit that omits the contribution of homogeneous photolysis, 1.5 mM formate (C^{+II}) to C^{+IV} implies 0.4 mM TOC has an average carbon oxidation state of −5.5, a chemically unrealistic value. An alternative electron acceptor is therefore needed. If instead a 50% loss is attributed to homogeneous photolysis (control B), then (0.5)(1.9) yield of 0.4 mM TOC implies a carbon oxidation state of −0.75.

The data in Fig. 2 show a rapid decrease of S_T^{-II} in the presence of ZnS. Control experiments described in Table 4 demonstrate the occurrence of a heterogeneous photoelectrochemical reaction for the loss of S_T^{-II}. Comparison of the data in the presence and absence of ZnS shows that photoelectrochemical decomposition of S_T^{-II} is much more rapid than homogeneous photolysis. The direct photolysis of H_2S by ultraviolet irradiation is discussed by [20,21].

The loss of S_T^{-II} shown in Fig. 2 leads to the partial dissolution of the ZnS. Once the sulfide is exhausted, up to 10^{-4} M Zn^{2+}(aq) is released at pH 6.3 (data not shown). The saturation ratio given by Q/K_{sp} is nominally 8 after 160 min of irradiation, where $Q = [Zn^{2+}][S^{2-}]$ and K_{sp} is the solubility product of ZnS. This saturation ratio is qualitatively equivalent to unity when uncertainties in the acid dissociation constant of HS^- and in the solubility product of ZnS(s) are taken into account.

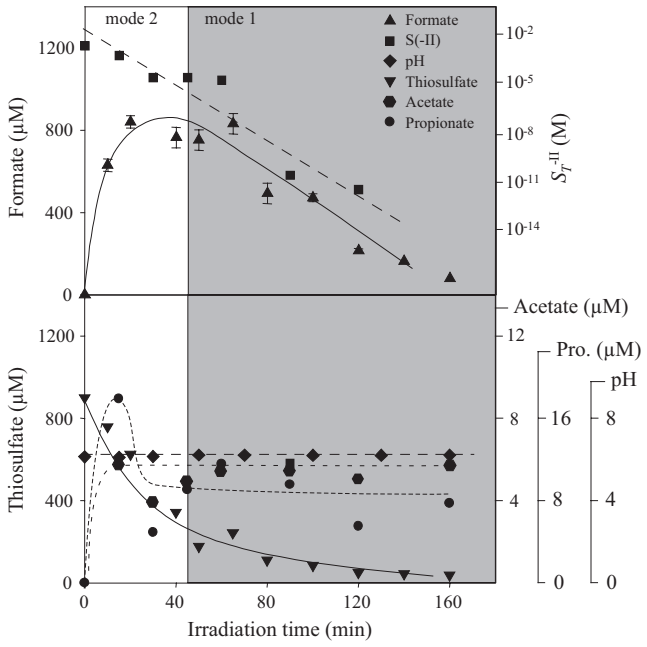

Fig. 3. Time profile of formate, acetate, priopionate, pH, S_T^{-II}, sulfate, and thiosulfate, concentrations during irradiation (mode 2 experiment). Lines are drawn to aid the eye and do not represent a model fit. *Initial conditions*: 33 mM C_T^{+IV} (CO_2 bubbling), 2.3 g L^{-1} ZnS (method 1), 2 mM sulfur hole scavenger, pH 6.3, 15 °C, and ultraviolet irradiation (200–400 nm).

3.2. Formate generation: photoreduction reactions with ZnS colloid

Formate is photoproduced from inorganic carbon C_T^{+IV} by ZnS when S_T^{-II} is present above 10^{-5} M, as shown in Fig. 3 from 0 to 40 min. This process is depicted by mode 2 in Fig. 1. After 40 min, S_T^{-II} is depleted, the reaction reverts to mode 1 (cf. Figs. 1 and 2), and the formate concentration decreases. The important role of S_T^{-II} is confirmed in a separate experiment in which the solution is spiked at 45 min with 4 mM of the sulfur hole scavenger solution. In this case, the formate concentration again increases (data not shown) until 60 min, after which time S_T^{-II} is again depleted and the formate concentra-

Table 4
Control experiments to demonstrate the occurrence of a heterogeneous photoelectrochemical reaction for the loss of S_T^{-III} in the presence of ultraviolet irradiation, colloidal ZnS particles, and formate

Description	Variables				Observation
	UV (λ < 410 nm)	Catalyst (ZnS(s))	S_T^{-II}	Formate	S_T^{-II} loss
Photochemical reaction 2	Yes	Yes	Yes	Yes	Yes (100%)
Control F	No	Yes	Yes	Yes	No
Control G	Yes	No	Yes	Yes	Very slow (<1%)
Control H	Yes	Yes	No	Yes	No[a]
Control I	Yes	Yes	Yes	No	Yes (100%)
Control J	Yes	No	Yes	No	Slow (<10%)

Reaction conditions are described in the caption of Fig. 3. Percentages in parentheses indicate the relative initial rates.
[a] S_T^{-II} is not present within analytical uncertainty during irradiation.

Table 5
Control experiments to demonstrate the occurrence of a heterogeneous photoelectrochemical reaction (namely, mode 2 of Fig. 1) for the generation of formate in the presence of ultraviolet irradiation, colloidal ZnS particles, a sulfur hole scavenger, and a C_T^{+IV} electron scavenger

Description	Variables				Observation
	UV ($\lambda < 410$ nm)	Catalyst (ZnS(s))	Sulfur hole scavenger	C_T^{+IV} electron acceptor	Formate production
Photochemical reaction 3	Yes	Yes	Yes	Yes	Yes
Control K	No	Yes	Yes	Yes	No
Control L	Yes	No	Yes	Yes	No
Control M	Yes	Yes	No	Yes	No
Control N	Yes	Yes	Yes	No	No
Control O[a]	Yes	Zn^{2+}(aq)	No	Yes	No
Control P[b]	No	Yes	Yes	Yes	No

Reaction conditions are described in the caption of Fig. 3.
[a] 10^{-6} M $ZnSO_4$(aq) was used instead of colloidal ZnS(s). The sulfur hole scavenger also was not added so as to avoid the formation of ZnS(s) via precipitation of Zn^{2+}(aq).
[b] Experiment was done in the dark at 45 °C.

tion again goes down (i.e., the system reverts from mode 2 to mode 1).

Control experiments confirm that formate production is associated with the photoelectrochemistry of ZnS colloids (Table 5). No formate is detected in the absence of UV irradiation (control K), indicating that dark thermal chemistry is not the mechanism for the reaction. Formate is also not found when no colloidal ZnS particles are present (control L). The presence of both an electron donor (control M) and an electron acceptor (control N) is necessary for formate production. Homogenous photoreduction of formate by aqueous Zn^{2+} is ruled out because no formate production is observed when 10^{-6} $ZnSO_4$ solution is used instead of ZnS colloidal particles (control O). This test is motivated by measurements during the course of the reaction that show up to 10^{-6} M Zn^{2+}(aq) is released to aqueous solution at the same time as formate production takes place. Control P, done under the same conditions as control A except at 45 °C, shows that no formate is produced by thermal reaction. This control is necessary because the temperature of the top 1 cm of solution rises to 45 °C, i.e., the incomplete water jacket around the reactor delivers no cooling to this region while the rest of the solution remains at 15 °C.

The photochemical production of formate depends strongly on the pH of the solution (Fig. 4a). Lower pH favors formate production, at least over the range of $5.3 < pH < 9.3$. The initial formate production rate (calculated for the first 15 min of reaction) decreases by 65% for an increase of one pH unit over the range $6.3 < pH < 8.3$. At pH 9.3, the production of formate is below the detection limit after 160 min irradiation, thus setting an upper limit of 5×10^{-7} M min^{-1} at this pH for the initial formate production rate. The pH does not change during irradiation (e.g., see time series in Fig. 3).

The dependence of the initial formate production rate on pH approximately tracks the speciation of C_T^{+IV} as $H_2CO_3^*$ and S_T^{-II} as H_2S in a closed system (Fig. 4b), suggesting that surface concentration of one of these species could occur in the rate law of the limiting step. The isoelectric pH for the colloidal ZnS particles in nominally 1 mM Na_2S is 3.75 ± 0.25 (see Fig. A4 of appendix). The ZnS particles are therefore negatively charged in the pH-dependent studies over the range of $5.3 < pH < 9.3$, and negatively charged species such as HCO_3^- or HS^- face an electrostatic barrier to surface adsorption. These relationships suggest possible reactive surface species of >ZnS::CO_2 and >ZnS::H_2S. $H_2CO_3^*$ speciates as CO_2(aq) in a 600:1 ratio with H_2CO_3. Neutral sulfur oxyanions such as $H_2S_2O_3$ and H_2SO_3 are insignificant for $5.3 < pH < 9.3$. The abrupt switch

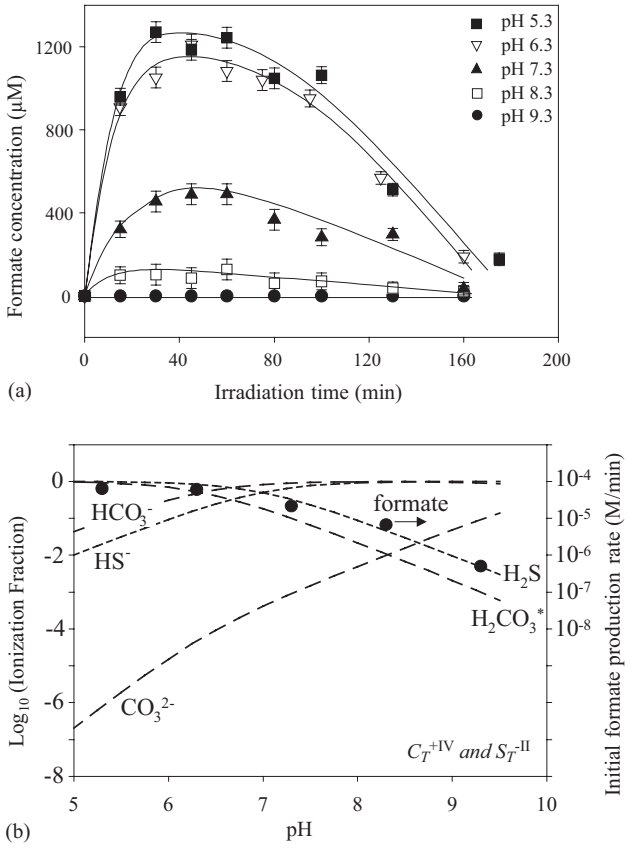

Fig. 4. (a) Time profile of formate concentration during irradiation for several pH values. *Initial conditions*: same as Fig. 3 except that C_T is set by $NaHCO_3$ addition. (b) Left-hand axis shows speciation of C_T^{+IV} as $H_2CO_3^*$, HCO_3^-, and CO_3^{2-} and S_T^{-II} as H_2S and HS^-. Right-hand axis shows initial production rate of formate (log axis).

from mode 2 to mode 1 after 40 min of irradiation also tracks closely with the abrupt drop in S_T^{-II} from 10^{-4} to 10^{-6} M rather than the smooth loss of thiosulfate from 450 to 350 μM (Fig. 3). We therefore suggest that a sulfide species, rather than a sulfur oxyanion, is the predominant hole scavenger. As a test, varying the initial thiosulfate concentration from 0.50 to 1.4 mM through spiking experiments does not alter the formate production kinetics (data not shown). Even so, in the absence of spectroscopic evidence our assignments of >ZnS::CO_2 and >ZnS::H_2S as the reactive species are tentative. Another possibility that we cannot rule out is that outer-sphere electron transfer takes place and no surface-adsorbed species forms.

The experimental results show that both bubbling CO_2 and adding $NaHCO_3$ lead to formate production via ZnS-mediated photochemistry (shown in Fig. 3 for CO_2 bubbling; no data shown for $NaHCO_3$). In contrast, Kanemoto et al. [2] report that no products form when CO_2 bubbling is replaced by bicarbonate addition. The difference between our results and those of Kanemoto et al. may arise from the difference in pH values in the two sets of experiments: the addition of $NaHCO_3$ increases pH compared to CO_2 bubbling, which Kanemoto et al. do not appear to take into account. We find that there is no difference between using CO_2 or bicarbonate as the inorganic carbon source so long as other conditions are held constant. This result is consistent with the equilibration of aqueous HCO_3^- and dissolved CO_2 with one another in under 10 s at pH 6.3 [22], which can be compared to the 1 h timescale of the photochemical experiments. The agreement in results also suggests any possible impurities in the CO_2(g) or $NaHCO_3$(s) do not significantly affect our observations.

The initial production rate of formate is proportional to the concentration of the dissolved inorganic carbon, at least over the investigated range $0 < C_T^{+IV} < 65$ mM (Fig. 5). In these experiments, the amount of added $NaHCO_3$ is varied while pH is held at 6.3 by addition of sulfuric acid. Keeping in mind the finding that the putative reactive surface species is >ZnS::CO_2 and assuming that the reaction rate is first-order in [>ZnS::CO_2], we conclude that the linear relationship observed between the reaction rate and [CO_2(aq)] implies a linear relationship between [>ZnS::CO_2] and [CO_2(aq)]. In this case, the adsorption isotherm is in a subsaturated regime (e.g., the linear region of a Langmuir adsorption isotherm) even up to 65 mM C_T^{+IV}, which corresponds to 35 mM CO_2(aq) at pH 6.3. Both an electron scavenger such as >ZnS::CO_2 and a hole scavenger such as >ZnS::H_2S are necessary for the reaction, and the absence of saturation at high C_T^{+IV} suggests that H_2S and CO_2 do not compete for the same surface sites (i.e., competitive versus noncompetitive Langmuir–Hinshelwood mechanism). Another possibility is that one or both of the species remain dissolved instead of surface adsorbed and undergo outer-sphere electron transfer (i.e., Eley–Rideal mechanism).

Quantum efficiency is the rate of product formation divided by the light intensity extinguished. Our experimental results show that the quantum efficiency of initial formate production is 10%, which demonstrates that colloidal ZnS is an efficient photocatalyst [1]. Quantum efficiency is a lower limit of the quantum yield because light is extinguished both by absorption from the photocatalyst and by light scattering from the particle suspension. This quantum efficiency is greater than the value of 4% reported previously for MnS [16].

3.3. Different sample preparation methods (method 1 versus method 2)

To explore how the results depend on the nature of the ZnS particles, we conducted photochemical experiments with ZnS suspensions that had not and had been aged, namely methods 1 and 2. Similar time profiles of formate production were observed for the two suspensions (Fig. 6). Therefore, the aging process, which affects crystallite size, the number and types of defects, and the reconstruction of the surface, does not appear to affect the ultimate photoelectrochemical reactivity, at least for the two suspensions studied. Unlike thermal catalysis, photocatalytic reactions are not directly proportional to specific surface area because the rate-limiting step is photon absorption [1].

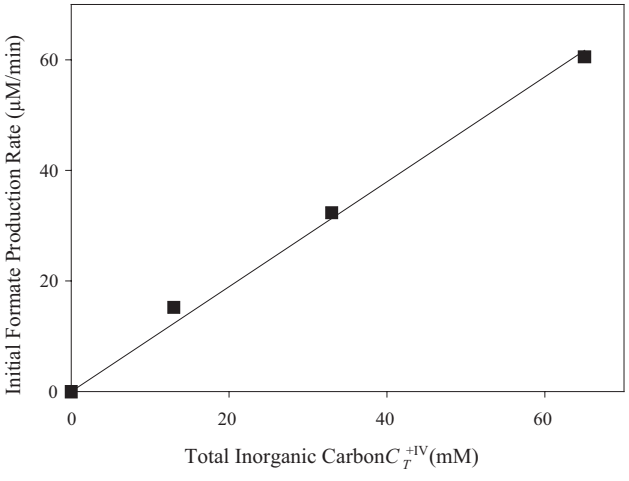

Fig. 5. Dependence of the initial production rate of formate on the initial value of C_T^{+IV}. *Initial conditions*: same as Fig. 3 except that C_T is set by $NaHCO_3$ addition.

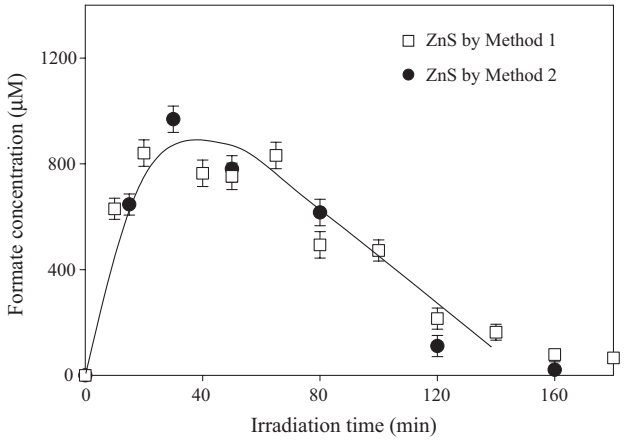

Fig. 6. Time profile of formate concentration during irradiation for ZnS suspensions prepared by methods 1 and 2. *Initial conditions*: same as Fig. 3.

3.4. Carbon–carbon coupling reactions with ZnS colloid

The conduction-band electrons of ZnS lead to the formation of carbon–carbon products. The initial carbon–carbon products arise from the coupling reactions of formate and therefore lead to C_2 compounds, such as acetate. Later in the irradiation, the possible permutations of coupling reactions are much more numerous, such as C_1 with C_2 or C_2 with C_2 and so on. The data in Fig. 3 show the presence of acetate and propionate in both mode-1 and mode-2 regimes. At 160 min when formate is no longer present, the concentration of total organic carbon is 2.0 mg L^{-1}. Acetate and propionate account for 0.7 mg L^{-1}. The remaining 1.3 mg L^{-1} is hypothesized by us to include molecules having carbon–carbon chains longer than C_3.

A possibility is that significant quantities of organic material adsorb to the surface of the ZnS particles. If so, this material would not pass through the syringe filter, and the reported TOC yield of 2.0 mg L^{-1} would be understated. To test for this possibility, we analyze filtered and dried ZnS particles after photochemistry by the TOC solids method. No organic carbon is detected. The detection limit of the method, which is 0.5 mg C in 1 g sample, implies an upper limit of 1 mg L^{-1} undetected adsorbed carbon based upon a colloid loading of 2.3 g L^{-1}. Therefore, we cannot rule out that our apparent yield of 2.0 mg L^{-1} TOC could be understated by up to 50%.

An additional possibility is that adsorbed carbon could affect the surface chemistry, thus causing a change in reactivity as carbon–carbon products form. The absence of detected solid TOC, in conjunction with the above stated detection limit, implies upper limits of 2.6×10^{-5} to 9.0×10^{-2} of fractional monolayer coverage by adsorbed carbon–carbon products assuming a limiting condition of monodisperse colloidal particle sizes from 10 to 600 nm. This calculation is based upon the cross-sectional area of HCHO (1.9 $Å^2$ $molec^{-1}$), the density of ZnS (4.0×10^3 kg m^{-3}), and particle diameters ranging from 10 nm (Fig. A2a) to 600 nm (Fig. A3a for pH of 6.3). (Supermicron particles apparent in the TEM images of Fig. A2b and in the DLS measurements of Fig. A3b make only a small contribution to the overall surface area of the colloidal suspension.) The highest estimated fractional monolayer coverage of 0.09 still suggests a limited role for adsorbed carbon–carbon products in altering reactivity, although attachment to active sites on the surface cannot be entirely ruled out.

4. Conclusions and implications for prebiotic synthesis

The results of this paper show that inorganic carbon is photoreduced to form organic molecules such as formate, acetate, and propionate in the presence of irradiated ZnS colloids (mode 2, Fig. 1). In the absence of hole scavengers, photooxidation of organic molecules also occurs (mode 1, Fig. 1). Photochemically induced redox chemistry of this type could have assembled building blocks in the prebiotic synthesis of even more organized molecules (e.g., membrane structures) on the early Earth. Factors influencing the prevalence of this chemistry in the Hadean were the occurrence of the photocatalyst, its quantum efficiency, and the reaction conditions.

There is currently no scientific consensus regarding the mechanisms that could have produced prebiotic molecules over a wide range of conditions on early Earth. Proposals are that organic molecules may have originated via spark discharge (lightning) [23,24], hydrothermal vents [7,25,26], or cometary delivery [27–31]. It remains important to consider alternative mechanisms, such as photoelectrochemistry on mineral colloids. Synergistic combinations of these several mechanisms may also have been active.

Acknowledgment

This study is supported by the National Aeronautics and Space Administration under Grant NAG5-13472 issued through the Office of Space Science.

Appendix A. Sample characterization

Slurry samples were dried, powdered, and mounted on glass slides for characterizing the ZnS atomic structure by X-ray diffraction. Powder patterns were collected using a Scintag PADx Diffractometer equipped with graphite-monochromatized Cu $K\alpha_1$ radiation ($\lambda = 1.5405$ Å). The scanning rate was 1.0° min^{-1} between 2θ value of 10° and 80°.

The XRD diffraction patterns (Fig. A1) were consistent with the formation of cubic ZnS (sphalerite) powders. Namely, the lattice constants of 5.38 ± 0.005 and 5.39 ± 0.006 Å for ZnS prepared by methods 1 and 2, respectively, compare well with the value of 5.406 Å for sphalerite ZnS in the JCPDS Powder Diffraction File No. 5-566.

Concurrent particle sizing and surface charge measurements were performed using dynamic light scattering (DLS) [32]. The instrument was a Brookhaven Instruments Corporation 90Plus/BI-MAS Particle Size Analyzer equipped with Phase Analysis Light Scattering technology for the determination of surface charge [33]. Particle sizing by DLS is a noninvasive technique whereby the diffusion of particles in solution is measured through light scattering. As a result, the samples were examined under aqueous conditions. Possible changes in the surface,

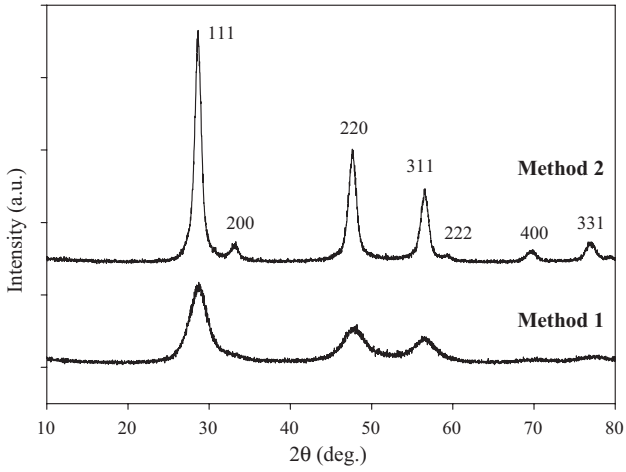

Fig. A1. X-ray diffraction patterns of the synthesized ZnS particles.

which can result from oxidation during filtering and drying for other sizing methods such as electron microscopy, were thus avoided.

Particle size and surface charge were determined by analysis of scattered light. The intensity correlation function of each sample was measured over five runs at a scattering angle of 90° from the incident laser beam (695 nm). Particle sizes from 5 to 3000 nm were determined from the autocorrelation function based upon the CONTIN [34] and Non-Negative Least Squares [35] analysis procedures. The electrophoretic mobilities were determined by measuring the frequency shift of the scattered light as the particles moved in an applied electric field. The scattered light was frequency shifted by the Doppler effect and, given that the direction of the electric field was known, both the sign (positive or negative) and the magnitude of the electrophoretic mobility and hence surface charge were determined.

These sizing and surface charge methods were applied to colloidal ZnS particles present in the supernatant of the third centrifuge–decant–resuspend cycle described in Section 2.1.2. Specifically, 1 mL of the supernatant was diluted in 70 mL of 1 mM sulfide rinse solution, resulting in a pH of 12.3 ± 0.2. pH-dependent measurements were carried out by the addition of HCl (0.02 M) to the diluted colloidal solution prior to DLS analysis. Sample temperature was controlled at 298 K by the instrument. Anoxic conditions were maintained during the manipulations.

Transmission electron microscopy (TEM) was also employed as an alternative sizing approach. ZnS particles in suspension were transferred under anoxic conditions to 300-mesh 3-mm carbon-coated copper grids having a Formvar backing. The particle-laden grids were dried under a stream of N_2 and then capped under anoxic conditions in glass vials for transport to the electron microscope. During transfer from the vials to a beryllium TEM sample holder, the grids were exposed to atmospheric oxygen for less than one minute, after which they were under high vacuum in the microscope. Imaging was performed using a Philips CM12 scanning TEM with a high brightness (LaB_6) electron gun.

The three complementary techniques (XRD, TEM, and DLS) were employed to characterize the size distribution of the powders. The broadness of the XRD diffraction peaks (Fig. A1) for the freshly precipitated material (method 1) indicated a lack of long-range ordering and implied crystallite sizes smaller than 1 μm. In comparison, the sharper diffraction peaks for aged ZnS (method 2) indicated a growth in crystallite size. The base of the diffraction peaks for the aged material, however, remained broad, which suggested a residuum of small crystallites was still present even after aging. A multimodal particle size distribution was thus implicated. The TEM images corroborated the presence of nanoscale, poorly crystalline ZnS in the fresh precipitate (Fig. A2a) and a mixture of nanoscale ZnS and micron-size hexagonal ZnS particles in the aged material (Fig. A2b).

Unlike the dry powders analyzed in the XRD and TEM methods, the DLS measurements were performed for aqueous suspensions and thus the size distributions should have been unaltered from those of the photochemical experiments. The DLS measurements indicated that the particle size distributions had two

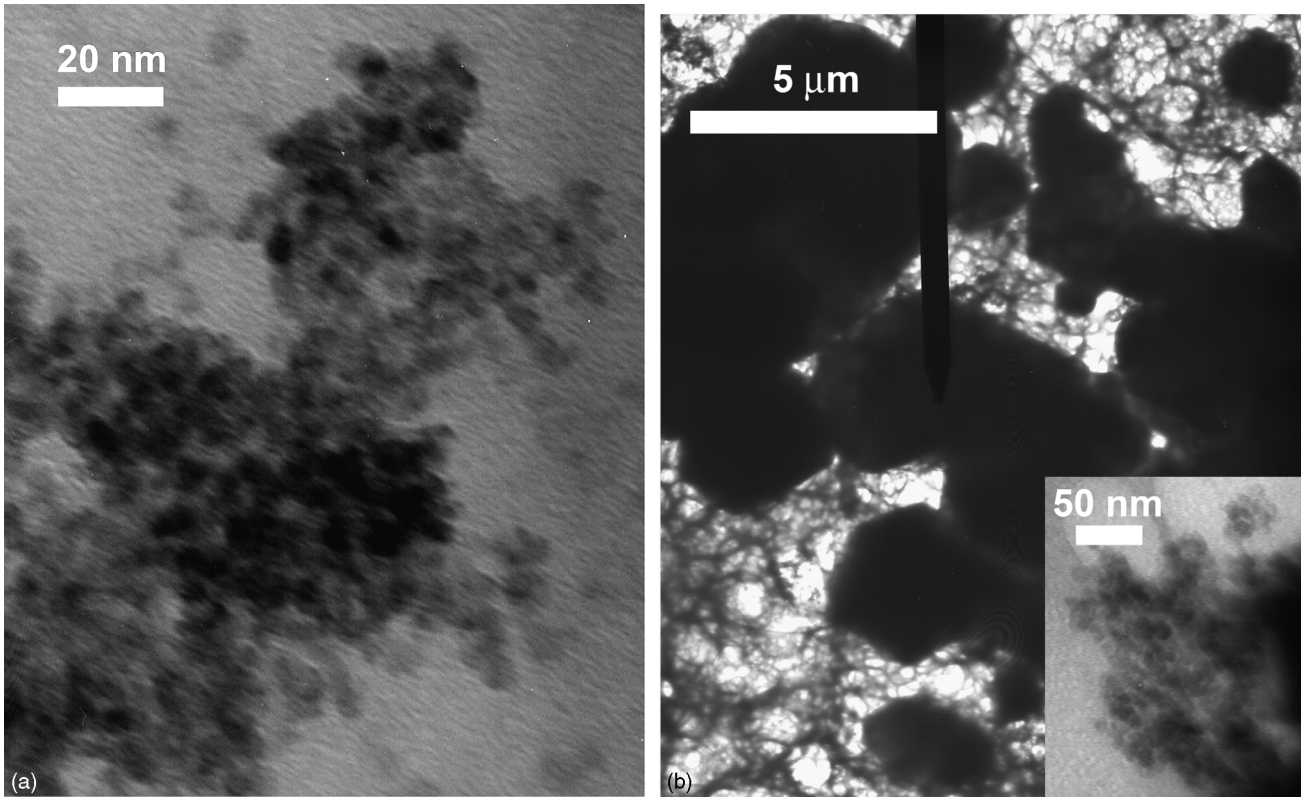

Fig. A2. Transmission electron micrographs of the synthesized ZnS particles. (a) ZnS prepared by method 1. (b) ZnS prepared by method 2. *Inset*: nanoscale ZnS particles are present in the suspensions prepared by method 2.

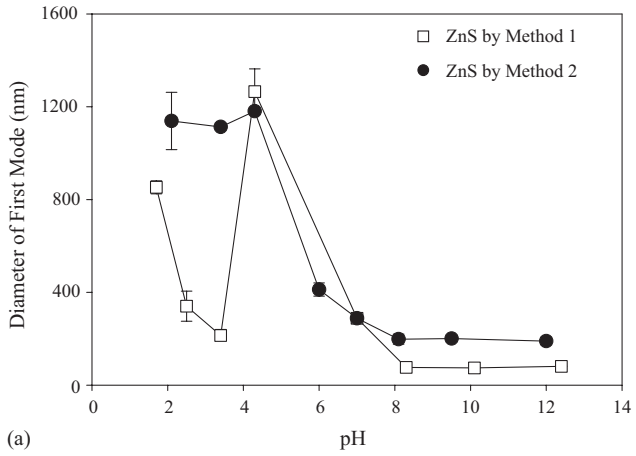

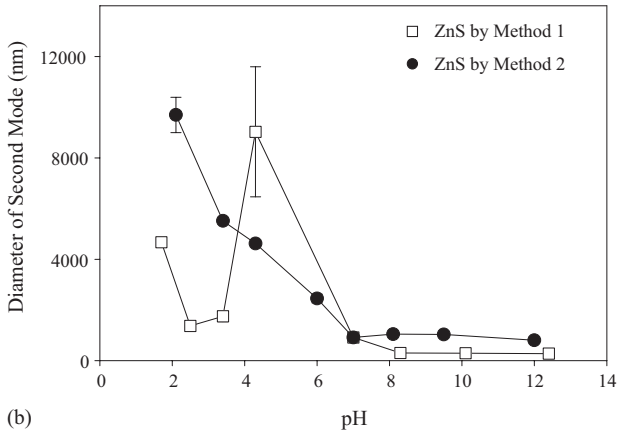

Fig. A3. pH-dependent mode diameters of the particle size distribution of the synthesized ZnS colloids. The particle size distributions have two modes, which are shown in (a) and (b). The mode diameters are determined by inversion of the DLS measurements of the ZnS colloids.

modes (Fig. A3a and b). Namely, above pH of 8, ZnS prepared by method 1 has modal diameters of 50 and 400 nm, which increased to 200 and 1000 nm, respectively, for aged material prepared by method 2. The modal diameters were determined by inversion of the DLS measurements of the ZnS colloids using intensity-weighted, multimodal models [32,34,35].

Whereas the TEM measurements showed individual crystallites, light scattering was sensitive to the extent of particle flocculation. Consistency with the TEM measurements required that the 400-nm mode diameter measured for method 1 arise from the flocculation of nanoscale particles. In contrast, the population centered around 1000 nm for method 2 may have been dispersed single crystals while still being consistent with the TEM images (Fig. A2b). For both methods, the modal diameters increased for decreasing pH, indicating that flocculation increased, which commonly occurs as net surface charge on the particles diminishes. Therefore, for the conditions of the photochemical experiments (i.e., pH of 6.3), flocs composed of primary crystallites of tens to hundreds of nm best described the particle size distribution of method 1. In comparison, for method 2, the particle suspension contained a combination of flocs of nanoparticles and of micron-sized hexagonal crystals.

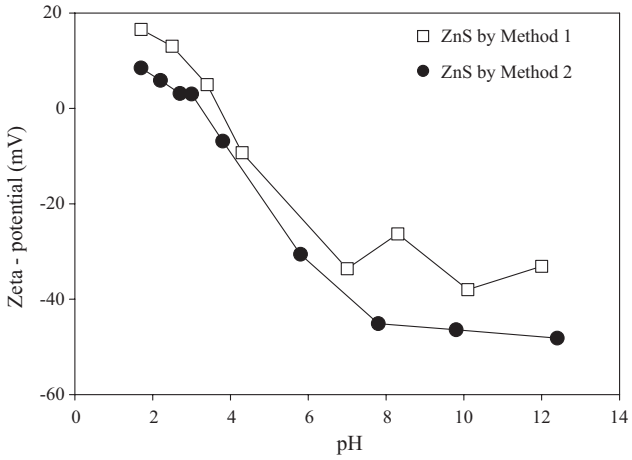

Fig. A4. Zeta potential as a function of pH for the synthesized ZnS colloidal particles.

The zeta potential measurements (Fig. A4) showed that the isoelectric point (pH_{iep}) for the colloidal ZnS particles was between 3 and 4 in nominally 1 mM Na_2S for particles prepared by both methods 1 and 2 [36]. The ZnS particles were therefore negatively charged for pH > 4, which was consistent with the results of [36].

References

[1] M.R. Hoffmann, S.T. Martin, W.Y. Choi, D.W. Bahnemann, Chem. Rev. 95 (1995) 69–96.
[2] M. Kanemoto, T. Shiragami, C.J. Pac, S. Yanagida, J. Phys. Chem. 96 (1992) 3521–3526.
[3] M. Anpo, H. Yamashita, Y. Ichihashi, S. Ehara, J. Electroanal. Chem. 396 (1995) 21–26.
[4] T. Inoue, A. Fujishima, S. Konishi, K. Honda, Nature 277 (1979) 637–638.
[5] B.R. Eggins, P.K.J. Robertson, E.P. Murphy, E. Woods, J.T.S. Irvine, J. Photochem. Photobiol. A-Chem. 118 (1998) 31–40.
[6] H.D. Holland, The Chemical Evolution of the Atmosphere and Oceans, Princeton University Press, Princeton, NJ, 1984.
[7] N.G. Holm, Orig. Life Evol. Biosph. 22 (1992) 5–14.
[8] B.R. Eggins, P.K.J. Robertson, J.H. Stewart, E. Woods, J. Chem. Soc.-Chem. Commun. 4 (1993) 349–350.
[9] A. Henglein, M. Gutierrez, C.H. Fischer, Phys. Chem. Chem. Phys. 88 (1984) 170–175.
[10] P. Johne, H. Kisch, J. Photochem. Photobiol. A-Chem. 111 (1997) 223–228.
[11] J.W. Morse, F.T. Mackenzie, Aquat. Geochem. 4 (1998) 301–319.
[12] H.D. Holland, in: H.D. Holland, K.K. Turekian (Eds.), Treatise on Geochemistry, vol. 6, Elsevier/Pergamon, Amsterdam, 2004, p. 589.
[13] W.B. Yang, H.D. Holland, R. Rye, Geochim. Cosmochim. Acta 66 (2002) 3707–3718.
[14] I.B. Butler, M.A.A. Schoonen, D.T. Rickard, Talanta 41 (1994) 211–215.
[15] CRC Handbook of Chemistry and Physics, 75th ed., CRC Press, 1994, pp. 4–144.
[16] X.V. Zhang, S.T. Martin, C.M. Friend, M.A.A. Schoonen, H.D. Holland, J. Am. Chem. Soc. 126 (2004) 11247–11253.
[17] W. Stumm, J.J. Morgan, Aquatic Chemistry, Wiley, New York, 1996.
[18] L.S. Clescerl, A.E. Greenberg, A.D. Eaton, Standard Methods for Examination of Water & Wastewater, 20th ed., American Public Health Association, Washington, DC, 1999.
[19] J. Lundell, M. Rasanen, J. Mol. Struct. 437 (1997) 349–358.
[20] C.A. Linkous, C.P. Huang, J.R. Fowler, J. Photochem. Photobiol. A-Chem. 168 (2004) 153–160.
[21] G.R. Woolley, R.J. Cvetanov, J. Chem. Phys. 50 (1969) 4697.

[22] F.M.M. Morel, J.G. Hering, Principles and Applications of Aquatic Chemistry, Wiley, New York, 1993.
[23] S.L. Miller, Science 117 (1953) 528–529.
[24] S.L. Miller, H.C. Urey, Science 130 (1959) 245–251.
[25] N.G. Holm, J.L. Charlou, Earth Planet. Sci. Lett. 191 (2001) 1–8.
[26] J.B. Corliss, Nature 347 (1990) 624.
[27] J. Oro, Nature 190 (1961) 389–390.
[28] C. Chyba, C. Sagan, Nature 355 (1992) 125–132.
[29] C.F. Chyba, P.J. Thomas, L. Brookshaw, C. Sagan, Science 249 (1990) 366–373.
[30] C.F. Chyba, Nature 343 (1990) 129–133.
[31] E. Anders, Nature 342 (1989) 255–257.
[32] B. Chu, Laser Light Scattering, Academic Press, Boston, 1991.
[33] F. McNeil-Watson, W. Tscharnuter, J. Miller, Colloids Surf., A 140 (1998) 53–57.
[34] S.W. Provencher, Comput. Phys. Commun. 27 (1982) 213–227.
[35] I.D. Morrison, E.F. Grabowski, C.A. Herb, Langmuir 1 (1985) 496–501.
[36] J. Bebié, M.A.A. Schoonen, D.R. Strongin, M. Fuhrmann, Geochim. Cosmochim. Acta 62 (1998) 633–642.